Boron oxides: Ab initio studies with natural bond orbital analysis

A. V. Nemukhin and F. Weinhold

Citation: J. Chem. Phys. **98**, 1329 (1993); doi: 10.1063/1.464299
View online: http://dx.doi.org/10.1063/1.464299
View Table of Contents: http://jcp.aip.org/resource/1/JCPSA6/v98/i2
Published by the American Institute of Physics.

Boron oxides: *Ab initio* studies with natural bond orbital analysis

A. V. Nemukhin[a] and F. Weinhold
Theoretical Chemistry Institute and Department of Chemistry, University of Wisconsin, Madison, Wisconsin 53706

(Received 30 July 1992; accepted 2 October 1992)

We employ *ab initio* theory and natural bond orbital (NBO) analysis to describe the structure, energetics, vibrational properties, and bonding in small boron oxides, B_mO_n, supplementing recent studies on isovalent aluminum oxide clusters, Al_2O_n, in order to extend the overview of bonding tendencies in group IIIA metal oxides. The comparison of analogous boron and aluminum species reveals many surprising differences, such as the V-shaped (M=B) vs linear (M=Al) geometry of M_2O_3, the altered tendency toward cyclic structures (higher for M_2O_2 with M=Al, for M_3O_3 with M=B), and the diminished role of electron correlation in the boron congeners. Correlation effects are examined by a recently introduced selective, localized multiconfigurational approach. Differences in bonding patterns are traced to basic hybridization and electronegativity shifts (reduced ionic character of B–O vs Al–O bond). Detailed comparisons with recent experimental B_mO_n data (including isotopomer ir shifts) provide additional support for theoretical assignments in corresponding aluminum species, where significant disagreements between theory and experiment persist.

I. INTRODUCTION

Recent *ab initio* studies[1] on aluminum oxide molecules, Al_2O_n (n=1–4), performed at Hartree–Fock and correlated levels (typically, MP2/6–31G*) with natural bond orbital (NBO) analysis, revealed many interesting features of these compounds. In spite of the fact that for the corresponding boron oxide species several high quality calculations are known, we decided to reinvestigate some of the B_mO_n molecules, first, in order to draw out comparisons with the isovalent Al_mO_n species, and second, to estimate more precisely the quality of our predictions for the spectral properties of these molecules, since for the boron oxides new reliable experimental data have been reported recently.[2,3] We also wish to provide additional tests of a recently proposed technique[4] for incorporating NBOs into multiconfigurational wave functions to treat electron correlation effects in a highly selective, localized manner. All calculations were carried out with the GAUSSIAN 90 program system[5] with the accompanying NBO routines.[6]

II. GEOMETRIES, ENERGETICS, AND VIBRATIONAL SPECTRA OF B_mO_n MOLECULES

A. B_2O

The most recent experimental characterization of the B_2O molecule has been performed by Andrews and Burkholder.[3] The matrix isolation studies of the products of reactions of boron atoms with water vapor allowed these workers to assign the band at 1420.5 cm^{-1} to the B_2O species (^{11}B and ^{16}O). The isotopic ratios $^{16/18}\mathscr{R}_O$ ($^{11}B_2{}^{16}O$ vs $^{11}B_2{}^{18}O$) and $^{10/11}\mathscr{R}_B$ ($^{10}B_2{}^{16}O$ vs $^{11}B_2{}^{16}O$) were measured to be $^{16/18}\mathscr{R}_O$=1.033 and $^{10/11}\mathscr{R}_B$=1.020, and the authors concluded that B_2O should be a nearly linear molecule of the structure B–O–B.

The results of previous *ab initio* calculations[7,8] are consistent with these structural conclusions. The molecule is predicted to be linear, with harmonic frequencies as shown in Table I. It was found that another possible isomer, namely, B–B–O, had much higher energy. Nevertheless, Devore, Woodward, and Gole[9] attempted to assign a chemiluminescent emission spectrum measured after oxidation of small boron clusters to such a nonsymmetrical species.

The results of our calculations at the RHF/6–31G*, MP2/6–31G*, and MP2/6–311G** levels are summarized in Table I, where the total energies, energy optimized B–O distances in the linear B–O–B arrangement, harmonic vibrational frequencies, and ir intensities are shown.

We can see that the molecule is characterized by a shallow potential surface along the bending coordinate (the corresponding frequency, ω_2, is softer than a typical torsional mode). At the highest level considered here, MP2/6–311G**, the computed frequency of the ir-active ω_3 mode (1456 cm^{-1}) is fairly close to the experimental value (1420.5 cm^{-1}), while the more practical MP2/6–31G* level gives an error of about 5%. The isotopic ratios computed with the MP2/6–31G* approach ($^{16/18}\mathscr{R}_O$=1.034 and $^{10/11}\mathscr{R}_B$=1.021) are both in accurate (±0.1%) agreement with experiment.

Comparison with the corresponding aluminum oxide, Al–O–Al, shows[1] that both linear molecules are quite flexible along the bending mode (frequencies less than 100 cm^{-1}). In both oxides electron correlation effects lead to an elongation of the distance to oxygen (a little greater for aluminum oxide), signifying the major role of left–right (or bonding–antibonding[4]) correlation.

[a]Permanent address: Department of Chemistry, Moscow State University, Moscow 119899 GSP, Russia.

 0021-9606/93/021329-7$06.00

TABLE I. Calculated energies, geometries and harmonic frequencies (unscaled) for the B–O–B molecule. The ir intensities (in km/mol) of the intense line (ω_3) are shown in parentheses below the corresponding frequency. The frequencies of the isotopomers at the bottom of the table have been computed at the MP2/6–31G* level.

Level	Energy (a.u.)	R_{B-O} (Å)	$\omega_1(\Sigma_g)$	$\omega_2(\Pi_u)$	$\omega_3(\Sigma_u)$
Ref. 7			1002		1545
Ref. 8			1087	83	1633
RHF/6–31G*	−124.167 960	1.313	1126	120	1585
					(1050)
MP2/6–31G*	−124.467 044	1.333	1052	111	1496
					(1037)
MP2/6–311G**	−124.561 760	1.329	1043	24	1456
					(1123)
$^{10}B^{16}O^{10}B$			1103	113	1527
$^{11}B^{18}O^{11}B$			1052	107	1447

B. B_2O_2

In the case of aluminum oxides, the species Al_2O_2 showed a variety of low-lying isomers of distinct electronic structure, including fairly unusual cyclic species.[1] The situation with the B_2O_2 species seems more ordinary. This molecule has been nicely characterized by Ruscic, Curtiss, and Berkowitz[10] both theoretically and experimentally. The photoelectron spectrum of B_2O_2 and *ab initio* calculations at the Hartree–Fock (STO-3G, 4–31G, 6–31G*) and MP3/6–31G* levels provide evidence that the lowest energy structure is a linear O–B–B–O arrangement. Other isomers, namely, linear B–O–B–O, and cyclic, almost square B_2O_2, are considerably higher in energy.

The ir spectra of the matrix-isolated products of reaction of boron atoms with molecular oxygen, obtained by Burkholder and Andrews,[2] have led to assignment of the band at 1898.9 cm^{-1} (^{11}B and ^{16}O) to the linear O–B–B–O species. The isotopic ratios $^{16/18}\mathcal{R}_{O_2}$ ($^{11}B_2{}^{16}O_2$ vs $^{11}B_2{}^{18}O_2$) and $^{10/11}\mathcal{R}_{B_2}$ ($^{10}B_2{}^{16}O_2$ vs $^{11}B_2{}^{16}O_2$) are measured to be 1.023 and 1.030, respectively. A complete set of experimental vibrational frequencies obtained from matrix isolation studies has been reported by Serebrennikov.[11]

Although recognizing that O–B–B–O is the thermodynamically more stable isomer, Doyle[12] has concluded that a nonsymmetric species $(B–O–B–O)^+$ is present in vapor from vitreous boron trioxide, as deduced from collision activated mass spectra. Andrews and Burkholder[3] have assigned the band at 1408 cm^{-1} (with the isotopic ratios $^{16/18}\mathcal{R}_{O_2}=1.034$ and $^{10/11}\mathcal{R}_{B_2}=1.019$) and the band at 2047.5 cm^{-1} (with $^{16/18}\mathcal{R}_{O_2}=1.016$ and $^{10/11}\mathcal{R}_{B_2}=1.034$) to the species B–O–B–O. Therefore, there is evidence that both isomers, O–B–B–O and B–O–B–O, may be observed under appropriate experimental conditions.

Table II contains the parameters for the O–B–B–O molecule, including those obtained in previous works. Our computed (MP2/6–31G*) isotopic ratios for the well characterized Σ_u vibration ($^{16/18}\mathcal{R}_{O_2}=1.024$ and $^{10/11}\mathcal{R}_{B_2}=1.029$) are practically identical to those reported by Burkhold and Andrews.[2] The overall agreement with

TABLE II. Experimental data and calculated energies (a.u.), distances (Å) and unscaled harmonic frequencies (cm^{-1}) for the O–B–B–O molecule. The ir intensities (in km/mol) of the intense lines are shown in parentheses below the corresponding frequencies. The frequencies of the isotopomers at the bottom of the table have been computed at the MP2/6–31G* level.

Level	Energy	R_{B-O}	R_{B-B}	$\omega_1(\Pi_u)$	$\omega_2(\Pi_g)$	$\omega_3(\Sigma_g)$	$\omega_4(\Sigma_u)$	$\omega_5(\Sigma_g)$
Exp.[a]				213	410	585	1897.8	2060
Exp.[b]							1898.9	
Calc.[c]				236	542	630	2089	2302
RHF/4–31G[d]	−198.895 94	1.196	1.631	236	547	639	2031	2253
MP3/6–31G*[d]	−199.683 75	1.201	1.647	216	432	628	2052	2222
RHF/6–31G*	−199.184 918	1.182	1.667	235	538	631	2131	2314
				(85)			(349)	
MP2/6–31G*	−199.714 432	1.218	1.636	215	501	625	1898	2073
				(41)			(40)	
$^{18}O–^{11}B–^{11}B–^{18}O$				210	498	598	1854	2042
$^{16}O–^{10}B–^{10}B–^{16}O$				221	523	633	1953	2147
$^{18}O–^{10}B–^{10}B–^{18}O$				216	520	605	1911	2118

[a]Reference 11.
[b]Reference 2.
[c]Reference 8.
[d]Reference 10.

TABLE III. Experimental data and calculated energies (a.u.), distances (Å) and unscaled harmonic frequencies (cm^{-1}) for the O–B–B–O molecule. The ir intensities (in km/mol) of the intense lines are shown in parentheses below the corresponding frequencies. The frequencies of the isotopomers at the bottom of the table have been computed at the MP2/6–31G* level.

Level	Energy	$R_{B_1-O_2}$	$R_{O_2-B_3}$	$R_{B_3-O_4}$	$\omega_1(\Pi)$	$\omega_2(\Pi)$	$\omega_3(\Sigma)$	$\omega_4(\Sigma)$	$\omega_5(\Sigma)$
Exp.[a]								1408	2047.5
Calc.[b]					172	557	852	1478	2224
RHF/4–31G[c]	−198.869 20	1.337	1.314	1.202	176	553	843	1458	2206
RHF/6–31G*	−199.153 177	1.306	1.311	1.190					
MP2/6–31G*	−199.650 728	1.317	1.332	1.220	50	478	828	1488	2123
						(53)		(516)	(597)
^{11}B–^{18}O–^{11}B–^{18}O					48	471	803	1437	2088
^{10}B–^{16}O–^{10}B–^{16}O					51	495	848	1517	2197

[a]Reference 3.
[b]Reference 8.
[c]Reference 10.

the data of Ref. 11 is also quite good except for the Π_g mode. It is interesting that the MP3/6–31G* frequencies of Ref. 10 differ noticeably from our MP2/6–31G* values.

Table III presents the same results for the B–O–B–O species. Again the calculated isotopic ratios ($^{16/18}\mathcal{R}_{O_2}$ = 1.036 for ω_4 and 1.019 for ω_5; $^{10/11}\mathcal{R}_{B_2}$=1.016 for ω_4 and 1.035 for ω_5) are in good agreement with the experimental data.[3] The frequencies themselves (ω_4 and ω_5) are also fairly close to the observed lines, the ~5% overestimate being rather typical of this level.

Table IV lists the total and relative energies of several stationary points on the potential surface of B_2O_2. It is somewhat surprising that the B–O–B–O isomer (which appears to lie about 40 kcal/mol above the stable O–B–B–O isomer at MP2/6–31G* level) can be observed in the matrix isolation experiments[3] and also in the gas phase.[12] We should also mention that, unlike Al_2O_2,[1] the B_2O_2 molecule does not show a variety of low-lying isomers. As shown in Table IV, local minima corresponding to "square" (D_{2h}) and "rhombic" (C_{2v}) cyclic B_2O_2 structures (cf. Ref. 1) are considerably higher in energy, not expected to be detectable experimentally. Also unlike the corresponding Al_2O_2 systems,[1] correlation effects do not seem to play a crucial role in altering the relative stability of the isomers (though they provide significant quantitative corrections). Overall, electron correlation effects in these boron species appear to be less important in altering the basic Hartree–Fock trends than in the "analogous" aluminum compounds.

TABLE IV. Calculated energies, E (a.u.), and relative energies with respect to O–B–B–O, ΔE (kcal/mol), for the stationary points on the B_2O_2 surface.

Species	Level	E	ΔE
O–B–B–O	RHF/6–31G*	−199.184 918	0.0
B–O–B–O	RHF/6–31G*	−199.153 177	20.0
B_2O_2, square	RHF/6–31G*	−199.050 185	84.5
B–O–O–B	RHF/6–31G*	−198.834 187	220.1
O–B–B–O	MP2/6–31G*	−199.714 432	0.0
B–O–B–O	MP2/6–31G*	−199.650 728	40.0
B_2O_2, square	MP2/6–31G*	−199.614 849	62.5
B_2O_2, rhombic	MP2/6–31G*	−199.371 770	215.0

C. B_2O_3

The structure of the B_2O_3 molecule has been the subject of considerable discussion (see, e.g., Ref. 13). It is now commonly accepted that a V-shaped model (C_{2v} symmetry)

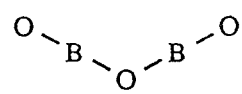

is the most stable arrangement. In recent matrix isolation spectroscopic studies, Burkholder and Andrews[2] assigned the band at 2062.3 cm^{-1} (^{11}B, ^{16}O) to this species. The reported isotopic ratios $^{16/18}\mathcal{R}_O$=1.019 and $^{10/11}\mathcal{R}_B$ =1.033 refer to the full isotopic substitutes (three oxygen or two boron atoms).

The energies and geometry parameters calculated in this work are compared with previous theoretical values[13] in Table V. This species presents an example of a floppy molecule with a shallow potential surface along the bending coordinate, and a correct description of the structure requires a sufficiently high theoretical level; we believe that the MP2/6–31G* approach is suitable for this purpose.

Vibrational properties of the B_2O_3 molecule are presented in Table VI. The calculated isotopic ratios, $^{16/18}\mathcal{R}_O$ =1.017 and $^{10/11}\mathcal{R}_B$=1.034, for the $\omega_9(B_2)$ mode are in excellent agreement with the experimental results[2] quoted above.

In addition to the interesting geometry change of the most stable B_2O_3 (V shaped) and Al_2O_3 (linear) isomer, it is noteworthy that B_2O_3 fails to exhibit the variety of low-lying isomeric forms found for Al_2O_3. We investigated a variety of other possible stationary points of B_2O_3 that might be suggested by analogy to aluminum structures, but no new points were found.

D. BO and B_3O_3

Although the importance of open-shell species in modeling the behavior of boron–oxygen mixtures is well recognized,[14] we did not systematically investigate the open-

TABLE V. Calculated energies and geometry parameters for the B_2O_3 molecule.

Level	Energy (a.u.)	$R_{O_c\text{-}B}$ (Å)	$R_{B\text{-}O_t}$ (Å)	∢(B–O_c–B)	∢(O_c–B–O_t)
RHF/4–21G*[a]	−273.625 04	1.324	1.188	136.0°	178.3°
RHF/6–31G*	−274.135 036	1.313	1.189	145.5°	180.0°
MP2/6–31G*	−274.830 577	1.334	1.221	136.1°	177.6°

[a]Reference 13.

shell boron oxides in the present work. However, two of these species, $(BO)_n$, $n=1$, 3, may be mentioned as representative.

The diatomic boron oxide molecule, BO, has been extensively studied previously.[15] At the UMP2/6–31G* level (comparable to the treatment used for closed-shell species), we found for the ground $^2\Sigma^+$ state of BO the calculated interatomic distance 1.216 Å and harmonic frequency 1936 cm^{-1}, with total energy E(UMP2) $=-99.762\,452$ a.u., which gives an impression of the accuracy at this level.

We also wish to report preliminary results for the interesting cyclic $(BO)_3$ system

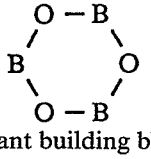

which is a very important building block of high molecular weight boron oxides in gaseous and solid phases,[12] and is typical of cyclic structures in compounds containing boron, oxygen, and hydrogen atoms.[16] The planar cyclic skeleton is a characteristic feature of both doublet and quartet states of this triradical species, which essentially places a single unpaired electron on each boron (cf. Sec. III). As shown in Table VII, the high-spin quartet state leads to a highly symmetric D_{3h} structure, but lies somewhat higher in energy (in nominal violation of Hund's rule). The lower-lying doublet species, with two α spins and one β spin, is slightly distorted to degenerate minima of C_s symmetry (which would be mixed by nonadiabatic coupling terms), but the essential character of the electronic distribution is otherwise unaltered. Table VII summarizes the structure and harmonic frequencies of these species, showing that they are both true minima on the UHF/6–31G* and UMP2/6–31G* potential energy surfaces. These triradical species apparently have no stable counterpart on the Al_3O_3 surface.

III. NBO ANALYSIS FOR THE B_mO_n SPECIES

The electronic structures of the lowest energy species, namely, BO, B–O–B, O–B–B–O, B–O–B–O, O–B–O–B–O, have been examined with the help of NBO analysis.[6] In each case geometry parameters optimized at the MP2/6–31G* level have been used, but corresponding Hartree–Fock wave functions were analyzed in order to carry out full NBO energetic analysis (including second-order perturbative estimates of NBO interaction energies). Since for these compounds correlation effects do not play a crucial role in predicting structural properties, we have not compared NBO's at the Hartree–Fock and correlated levels (as for aluminum oxides[1]).

The optimal NBO Lewis structures for the B_mO_n molecules are depicted in Fig. 1. Table VIII shows natural atomic charges and natural electron configurations (NEC) deduced from natural population analysis, while Table IX shows details of the NBO energies, occupancies, and composition for representative species.

In general, electronic delocalization is found to be significantly less important in the boron oxides than in corresponding aluminum species, with the departures from an idealized localized NBO Lewis structure ("non-Lewis density") typically amounting to 1% or less (vs ~5% for Al).

M≡O triple bonding is seen to be a ubiquitous feature of the boron oxide NBO Lewis structures, as in the corresponding aluminum species. However, one can recognize from Tables VIII and IX that the B–O bonds are of sig-

TABLE VI. Unscaled harmonic frequencies (cm^{-1}) for the B_2O_3 molecule. Infrared intensities (km/mol) for the intense lines are given in parentheses below corresponding frequencies. The frequencies of the isotopomers are calculated with the MP2/6–31G* approximation.

Level	$\omega_1(A_1)$	$\omega_2(B_2)$	$\omega_3(A_2)$	$\omega_4(B_1)$	$\omega_5(A_1)$	$\omega_6(A_1)$	$\omega_7(B_2)$	$\omega_8(A_1)$	$\omega_9(B_2)$
Exp.[a]									2062.3
Calc.[b]	108	491	462	518	597	817	1308	2314	2293
RHF/6–31G*	79	501	508	552	583	779	1356	2272	2283
MP2/6–31G*	87	456	466	488	529	756	1227	2100	2125
	(8)	(12)		(101)	(75)	(14)	(109)	(34)	(964)
$^{11}B_2{}^{18}O_3$	83	452	462	479	521	719	1157	2069	2089
$^{10}B_2{}^{16}O_3$	87	475	485	504	548	761	1227	2175	2197

[a]Reference 2.
[b]Reference 13.

TABLE VII. Calculated energies, B–O distances (R), and harmonic frequencies for the $(BO)_3$ molecule in doublet (^2C_s) and quartet ($^4D_{3h}$) geometries at uncorrelated (UHF/6–31G*) and correlated (UMP2/6–31G*) levels of theory. In $^4D_{3h}$ geometry, the symmetries of vibrational bands are successively (from lowest upward) E'', A_2'', E', A_1', A_1', E', A_2', E', with only the latter having strong ir intensity (MP2: 863 km/mol).

Species/Level		Energy (a.u.)	R (Å)	Frequencies (cm^{-1})
^2C_s	UHF	−298.762 487	1.36	266,282,496,562,565,861,1078,1196,1198,1237,1441,1458
	MP2	−299.466 787	1.38	236,260,468,515,519,776,1012,1116,1119,1154,1350,1380
$^4D_{3h}$	UHF	−298.759 726	1.3601	263(2),490,569(2),867,1086,1205(2),1245,1469(2)
	MP2	−299.437 671	1.3791	225(2),459,522(2),782,1021,1131(2),1147,1388(2)

nificantly higher covalency than corresponding Al–O bonds (as would be expected from the relative electronegativity differences). Thus the percentage of metal character in M–O bonds approaches 20% for the boron compounds (vs ~5% for Al). The increased triple-bond character of B_mO_n species is also manifested in the conspicuously higher frequencies of B–O vs Al–O stretching modes (viz., 1496 vs 988 cm^{-1} for the asymmetric stretch ω_3 of B–O–B vs Al–O–Al at the MP2/6–31G* level).

Reduced ionic character is most directly apparent in the calculated natural atomic charges (Table VIII). These tend to be close to B^+, O^- in the boron oxides, whereas much higher charges (approaching idealized Al^{3+}, O^{2-} ionic limits) were common in corresponding Al compounds. As in aluminum species, one can recognize a tendency toward higher ionic character in "interior" regions than at "end" positions, suggesting a characteristic difference between surface and bulk ionic character in extended phases.

One consequence of the reduced ionicity of boron oxides is that "alternating" structures (–M–O–M–O–) which avoid like-atom contacts are less strongly favored than in the aluminum oxides. Thus the linear O–B–B–O is actually the more stable minimum on the B_2O_2 surface, as remarked above, whereas O–Al–Al–O is quite unstable (by ca. 200 kcal/mol) compared to O–Al–O–Al for Al_2O_2.

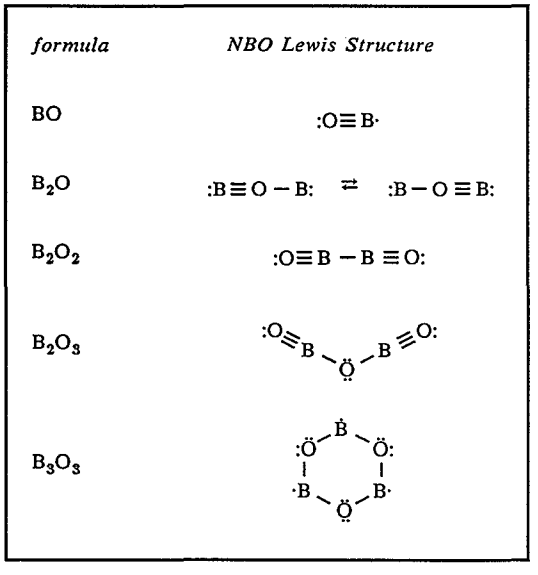

FIG. 1. NBO Lewis structures for ground state boron oxides.

Another interesting structural consequence of the reduced ionicity of boron oxides is seen in the V-shaped structure of B_2O_3 vs the linear structure of Al_2O_3. This can be rationalized in terms of elementary hybridization concepts. Although the formal Lewis structures are identical, the bonding hybrids of the central oxygen have significantly higher p character ($\sim sp^{1.3}$) in B_2O_3 (in accordance with Bent's rule), and the bond angle at O is therefore somewhat bent, in a manner resembling other covalent oxides (e.g., H_2O), rather than linear, as in the more highly ionic Al_2O_3. However, as the low frequency (ω_2) of the bending mode suggests, the central O_c hybrids of B_2O_3 still lie rather far from a nominal covalent limit, consistent with the gradual character of the ionic–covalent transition.

A similar argument accounts for the tendency toward four-membered ring structures for Al_2O_2 vs six-membered rings for B_3O_3

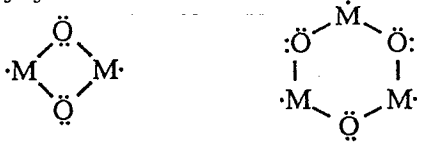

(M = Al) (M = B)

As the M–O electronegativity difference increases, the Bent's rule trend is toward pure p hybridization at M and pure s hybridization at O, both allowing for the ~90° bond angles of a nearly square arrangement, whereas for the sp^λ hybrids of more covalently bonded atoms, such 90° angles become increasingly strained.[17] Put another way, ions can adopt arrangements with ~90° contact angles, whereas co-

TABLE VIII. Natural population analysis of B_mO_n species at HF/6–31G* level (MP2/6–31G* optimized geometries), showing natural atomic charge (q) and effective valence shell natural electron configuration (NEC) of each atom.

Species	Atom	q	NEC
B–O	B	+0.9575	$2s^{1.82}2p^{5.11}$
	O	−0.9575	$2s^{0.84}2p^{1.18}$
B–O–B	B	+0.6452	$2s^{1.74}2p^{0.60}$
	O	−1.2903	$2s^{1.74}2p^{5.54}$
O–B–B–O	B	+0.8240	$2s^{0.73}2p^{1.42}$
	O	−0.8240	$2s^{1.74}2p^{5.05}$
O_t–B–O_c–B–O_t	B	+1.4107	$2s^{0.37}2p^{1.20}$
	O_t	−0.8958	$2s^{1.76}2p^{5.10}$
	O_c	−1.0298	$2s^{1.64}2p^{5.38}$
$(BO)_3$	B	+1.1018	$2s^{0.75}2p^{1.12}$
	O	−1.1018	$2s^{1.71}2p^{5.37}$

TABLE IX. List of principal NBOs for representative boron oxides (HF/6–31G* level, at MP2/6–31G* optimized geometries), showing orbital energy (in a.u.), occupancies (e), and composition ($c_B h_B + c_O h_O$) in terms of hybrids (h_B, h_O) and polarization coefficients (c_B, c_O) on each atom. For the open-shell B–O species, the upper entry is for α and the lower for β spin.

NBO type	E (a.u.)	Occ. (e)	Composition ($c_B h_B + c_O h_O$)
B–O			
σ(B–O)	−1.3535	1.0000	$0.422(sp^{2.09})_B + 0.907(sp^{0.88})_O$
	−1.3038	1.0000	$0.428(sp^{0.71})_B + 0.904(sp^{1.17})_O$
π(B–O)	−0.4960	1.0000	$0.481p_B + 0.877p_O$
	−0.5387	1.0000	$0.325p_B + 0.946p_O$
n(O)	−0.8855	0.9973	$sp^{1.11}$
	−0.9674	0.9926	$sp^{0.84}$
n(B)	−0.5452	0.9984	$sp^{0.47}$
	+0.1930	0.0078	$sp^{3.21}$
O–B–B–O			
σ(B–O)	−1.4920	1.9989	$0.459(sp^{1.43})_B + 0.889(sp^{0.67})_O$
π(B–O)	−0.5460	1.9942	$0.430p_B + 0.903p_O$
σ(B–B)	−0.7447	1.9960	$0.707(sp^{0.70})_B + 0.707(sp^{0.70})_B$
n(O)	−0.7034	1.8811	$sp^{1.46}$
O_t–B–O_c–B–O_t			
σ(B–O_c)	−1.3156	1.9893	$0.420(sp^{1.06})_B + 0.908(sp^{1.29})_O$
σ(B–$O)_t$	−1.3462	1.9948	$0.465(sp^{1.07})_B + 0.885(sp^{1.10})_O$
π_1(B–O_t)	−0.5958	1.9980	$0.413p_B + 0.911p_O$
π_2(B–O_t)	−0.5380	1.9983	$0.406p_B + 0.914p_O$
n_1(O_c)	−0.7034	1.8811	$sp^{7.01}$
n_2(O_c)	−0.6080	1.8586	p
n(O_t)	−0.9202	1.9819	$sp^{1.03}$
π_1^*(B–O_t)	+0.3400	0.0577	$0.911p_B - 0.413p_O$
π_2^*(B–O_t)	+0.2867	0.0680	$0.914p_B - 0.406p_O$

valently bonded atoms favor more open arrangements consistent with their directional sp^λ hybrids. The different preferred geometries of cyclic M_nO_m clusters (M=B vs Al) can thus be rationalized (via Bent's rule) in terms of reduced ionicity of B–O bonding.

For the B_2O_2 system we can demonstrate the advantages of the multiconfigurational NBO analysis[4] in explaining the features on the potential energy surface. Figure 2 shows the pathways for the dissociation of the linear isomers O–B–B–O and B–O–B–O (as discussed in the previous section, both species are probably detectable). As a reaction coordinate we have used either the distance between boron atoms, R_{B-B} (in the case of O–B–B–O), or the distance between central B and O atoms, R_{O-B}. At each point R_{B-B} or R_{O-B} all other geometry parameters have been energy optimized. The calculations have been carried out within the complete active space SCF (CASSCF) procedure while choosing the smallest expansion possible for the correct description of the dissociation to the two BO radicals. Only two orbitals responsible for qualitative changes in the electronic structure are included in the active spaces, and two electrons are allowed to occupy them. Namely, bonding and antibonding pairs of NBO's [σ(B–B) and σ^*(B–B) for O–B–B–O and σ(O–B) and σ^*(O–B) for O–B–B–O] are considered as active orbitals in accordance with our understanding of bond breaking: electrons are promoted into antibonding orbitals from the corresponding bonding orbitals.

In a sense, the curves of Fig. 2 present a minimal description of the dissociation pathways; only those correlation effects are taken into account which are needed in this particular application. Of course, in such modeling one could face a problem of radical changes of orbitals due to the SCF procedure. In this case we have checked that the changes go smoothly by performing the NBO analysis after the CASSCF orbitals are obtained and we are still within the limits of the same local minima in the orbital parameter spaces.

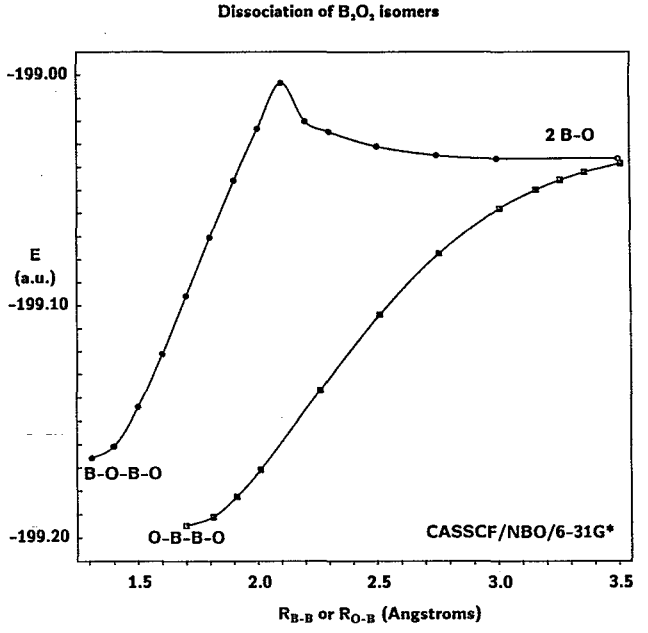

FIG. 2. Schematic potential energy curves [CASSCF/NBO(σ,σ^*)^2/6–31G*] for dissociation of B–O–B–O and O–B–B–O to 2B–O fragments, showing the avoided crossing barrier associated with reorganization of Lewis structure in the B–O–B–O case.

The usefulness of such an analysis can be recognized when looking at the changes in electronic structures along the dissociation pathways, Fig. 2. Obviously, in order to dissociate to two BO radicals from the B–O–B–O arrangement, the system must undergo a dramatic change in electronic arrangement (to move the unpaired spin from oxygen to boron on the left-hand fragment; cf. Fig. 1), which explains the presence of the potential barrier. The presence of a barrier in the B–O–B–O surface (vs the barrierless surface for O–B–B–O formation) suggests why different B_2O_2 isomeric products may be detected in different experimental arrangements, despite a significant difference in relative stability.

IV. CONCLUSION

Comparison of theoretical and experimental vibrational frequencies for boron oxides suggests that the MP2/6–31G* level provides a reasonably accurate and practical description of the oxides of group III elements. Since the experimental data are more extensive for B_mO_n than for analogous aluminum species, we consider the comparisons of the present work to provide support for the reliability of our previous theoretical predictions[1] for Al_mO_n species.

Comparison of boron and aluminum oxides on the basis of NBO and natural population analysis provides additional insight into structural differences that characterize these classes of compounds, due particularly to relative electronegativity differences. These comparisons clarify the electronic origins of observed differences in structural motifs (linear vs V shaped, four membered vs six membered, etc.) shifts of vibrational frequencies, and inverted relative stabilities of isomeric forms (O–M–O–M vs O–M–M–O, etc.) that distinguish boron and aluminum compounds.

Our results also illustrate the usefulness of the recently introduced CAS/NBO procedure[4] for describing electron correlation and bond dissociation. The localized NBO description allows one to clearly recognize the specific electronic rearrangements accompanying bond dissociation (typically leading to activation barriers), and the associated CAS/NBO procedure allows one to selectively treat the multiconfigurational aspects of such transition regions in an economical manner.

ACKNOWLEDGMENTS

We express appreciation to the Exchange Program between Moscow State University and UW-Madison which made this collaboration possible. This work was supported in part by the National Science Foundation Grant No. CHE-9007850.

[1] A. V. Nemukhin and F. Weinhold, J. Chem. Phys. (in press).
[2] T. R. Burkholder and L. Andrews, J. Chem. Phys. **95**, 8697 (1991).
[3] L. Andrews and T. R. Burkholder, J. Phys. Chem. **95**, 8554 (1991).
[4] A. V. Nemukhin and F. Weinhold, J. Chem. Phys. (in press).
[5] GAUSSIAN 90 program system, M. J. Frisch, M. Head-Gordon, G. W. Trucks, J. B. Foresman, H. B. Schlegel, K. Raghavachari, M. A. Robb, J. S. Binkley, C. Gonzalez, D. J. Defrees, D. J. Fox, R. A. Whiteside, R. Seeger, C. F. Melius, J. Baker, R. L. Martin, L. R. Kahn, J. J. P. Stewart, S. Topiol, and J. A. Pople (Gaussian, Inc., Pittsburgh, 1990). For the standard *ab initio* computational methods and basis-set designations employed throughout this work, see W. J. Hehre, L. Radom, P. v. R. Schleyer, and J. A. Pople, *Ab Initio Molecular Orbital Theory* (Wiley, New York, 1986).
[6] E. D. Glendening, A. E. Reed, J. E. Carpenter, and F. Weinhold, *NBO 3.0 Program Manual*, Univ. of Wisconsin Theoretical Chemistry Institute Report WIS-TCI-756 (1990), available through Quantum Chemistry Program Exchange (Department of Chemistry, Indiana University, Bloomington, IN) or Gaussian, Inc. (4415 Fifth Avenue, Pittsburgh, PA 15213); A. E. Reed, L. A. Curtiss, and F. Weinhold, Chem. Rev. **88**, 899 (1988).
[7] T. S. Zyubina, O. P. Charkin, A. S. Zyubin, and V. Zakzhevskii, Zh. Neorg. Khim. **27**, 558 (1982).
[8] H. Ginn, L. Jones, and D. Shillady, cited in Refs. 3 and 9.
[9] T. C. Devore, J. R. Woodward, and J. L. Gole, J. Phys. Chem. **92**, 6919 (1988).
[10] B. M. Ruscic, L. A. Curtiss, and J. Berkowitz, J. Chem. Phys. **80**, 3984 (1984).
[11] L. V. Serebrennikov, Vestnik Mosk. Univ. Khimia **22**, 606 (1981).
[12] R. J. Doyle, J. Am. Chem. Soc. **110**, 4120 (1988).
[13] H. Sellers, J. Boggs, A. V. Nemukhin, and J. Almlöf, J. Mol. Struct. (Theochem) **85**, 195 (1981).
[14] C. T. Stanton, N. L. Garland, and H. H. Nelson, J. Phys. Chem. **95**, 8741 (1991).
[15] A. V. Nemukhin, J. Almlöf, and A. Heiberg, Chem. Phys. **57**, 197 (1981).
[16] G. Mains, J. Phys. Chem. **95**, 5089 (1991).
[17] Bent's rule [H. Bent, Chem. Rev. **61**, 275 (1961)] in conjunction with the usual relationship between bond hybrids and bond angles [C. A. Coulson, *Valence*, 2nd ed. (Oxford University, New York, 1960), p. 204] predicts more open angles at electropositive B than at electronegative O, as is found ($\sphericalangle_{OBO}=121.04°$, $\sphericalangle_{BOB}=118.96°$ at MP2/6–31G* level).